Hearing Research 458 (2025) 109189

Contents lists available at ScienceDirect

Hearing Research

journal homepage: www.elsevier.com/locate/heares

Research paper

Narrow elliptical motion at the outer hair cell-Deiters' cell junction explains disparate features of uniaxial displacement measurements

Brian L. Frost [a,*], C. Elliott Strimbu [b], Elizabeth S. Olson [b,c]

[a] Howard Hughes Medical Institute and Laboratory of Sensory Neuroscience, the Rockefeller University, 1230 York Avenue, New York, 10065, NY, USA
[b] Columbia University Irving Medical Center, Department of Otolaryngology, Head and Neck Surgery, 180 Fort Washington Ave, New York, 10032, NY, USA
[c] Columbia University, Department of Biomedical Engineering, 1210 Amsterdam Ave, New York, 10027, NY, USA

ARTICLE INFO

Keywords:
Cochlear mechanics
Optical coherence tomography
Deiters' cell
Hair cell

ABSTRACT

Sound-evoked displacement responses at the outer hair cell-Deiters' cell junction (OHC-DC) are of significant interest in cochlear mechanics, as OHCs are believed to be in part responsible for active tuning enhancement and amplification. Motion in the cochlea is three-dimensional, and the architecture of the organ of Corti complex (OCC) suggests the presence and mechanical importance of all three components of motion. Optical coherence tomography (OCT) displacement measurements of OHC-DC motion from different experimental preparations often show disparate results, potentially due to OCT measuring only the motion component along the beam axis. In this work, we show that narrow elliptical motion at the OHC-DC – nearly along a straight line, where towards-base longitudinal motion is in phase with towards-scala-media transverse motion – can explain two such preparation-dependent differences. We present longitudinal and transverse components of displacement responses from the OHC-DC in the gerbil base in response to moderately high-level sound stimuli that exhibit precisely this *near-lineal motion*. The results show the potential for active longitudinal energy transfer in the OCC.

1. Introduction

Optical coherence tomography (OCT) has been used in recent years to measure motion within the organ of Corti complex (OCC), and a wealth of data from the base of the gerbil cochlea has been published (Dong et al., 2018; Cooper et al., 2018; Strimbu et al., 2018; Strimbu and Olson, 2022; Pierre et al., 2020; Cho and Puria, 2022; Strimbu et al., 2024). An early OCT study in the gerbil base by Cooper et al. (2018) showed that the motion in the region of the junction between outer hair cells (OHCs) and Deiters' cells (DC, and junction region is hereafter abbreviated OHC-DC) is larger than the motion in the rest of the OCC at most stimulus frequencies and sound pressure levels (SPLs). This region also exhibits broadband nonlinearity in response to multitone stimuli, which appears (at least in the cochlear base) to be highly localized, not affecting the basilar membrane (BM) or cells lateral to OHC-DC except at frequencies near the best frequency (BF). Under some experimental conditions the reticular lamina (RL) also does not exhibit sub-BF nonlinearity (Cho and Puria, 2022; Strimbu et al., 2024). This isolation from nonlinearity in the sub-BF region yields sharper tuning at BF in the BM and RL. How this occurs remains a central question of the study of cochlear mechanics.

While these features of OHC-DC region motion appear to be consistent across various studies, other quantitative features disagree between experiments. In particular, the OHC-DC phase responses relative to those of BM can differ greatly between experimental conditions. While all OHC-DC phase responses show phase accumulation characteristic of a traveling wave, some data show that OHC-DC leads BM across frequency, some show that it lags BM across frequency and some show that the two are in-phase in the BF region (Dong et al., 2018; Strimbu et al., 2018; Frost et al., 2022, 2023c,b; Strimbu et al., 2024). Meanwhile, the relative phase of OHC and BM motion remain foundational components of models that look to explain active cochlear tuning and amplification (Rabbitt, 2022; Rabbitt and Bione, 2023; Altoè et al., 2022). Synthesis of these apparently disparate data is required for the role of OHCs in cochlear function to be understood.

Two main factors leading to phase ambiguity in OCT motion measurement have been previously noted. The first is that along the axis of measurement, BM and OHC-DC may not lie in the same longitudinal cross-section (termed *skew*) (Cooper et al., 2018; Frost et al., 2022, 2023c). The second is that OCT-measured displacement responses are 1-D projections of a 3-D motion onto the beam axis — a direction

* Corresponding author.
E-mail address: bfrost@rockefeller.edu (B.L. Frost).

https://doi.org/10.1016/j.heares.2025.109189
Received 17 October 2024; Received in revised form 11 December 2024; Accepted 13 January 2025
Available online 23 January 2025

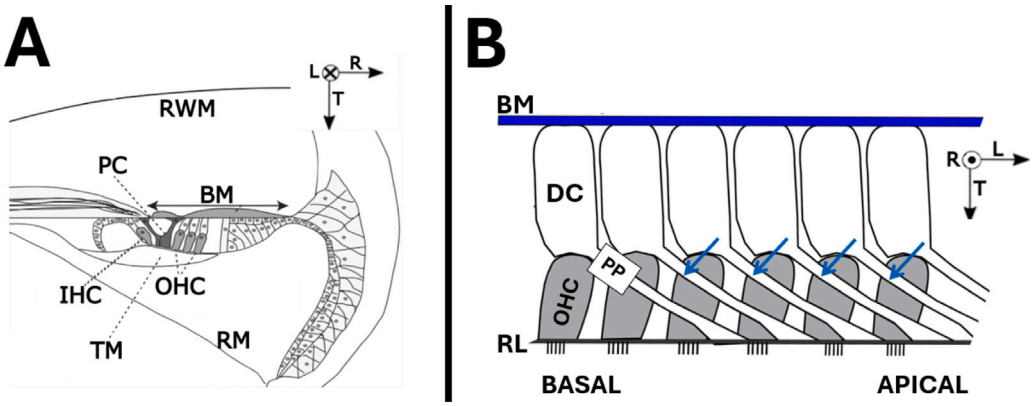

Fig. 1. Cartoons of the organ of Corti complex (OCC) viewed at two angles. Longitudinal, radial and transverse anatomical coordinate directions (L, R, T, respectively) are labeled at the top-right of each panel. Longitudinal points from base-to-apex, radial points from medial-to-lateral and transverse points towards scala media (SM). **A** – A radial-transverse cross-section of the OCC. RWM = Round Window Membrane, PC = Pillar Cells, BM = Basilar Membrane, IHCs = Inner Hair Cells, OHC = Outer Hair Cells, TM = Tectorial Membrane, RM = Reissner's Membrane. **B** – A longitudinal-transverse cross-section of the OCC through a row of OHCs. Blue arrows represent the approximate direction of OHC-DC motion previously measured by Frost et al. (2023c) DC = Deiters' Cells, PP = Phallangeal Processes, RL = Reticular Lamina.

with no inherent physiological meaning, that varies between experiments (Lee et al., 2016; Cooper et al., 2018; Frost et al., 2022, 2023c; Meenderink and Dong, 2022). As the motion of the OCC is in reality a 3-D vector field, it is not generally correct to say that there is "a phase response" at any given position. Each anatomical component of motion; longitudinal, radial and transverse, as marked in Fig. 1; may have a distinct phase response. This was noted by Cooper et al. (2018), who proposed that intra-OCC motion is elliptical, similar to what would be expected of fluid motion in the scalae (Lighthill, 1981, 1978). They found that when measuring through the round window membrane (RWM), OHC-DC phase led BM when the beam axis was pointed towards the apex but lagged BM when the beam axis was pointed towards the base. This behavior was also observed at a more apical location by Meenderink and Dong (Meenderink and Dong, 2022). A related finding has been noted by Frost et al. (2023c) and Strimbu et al. (2024), who showed that OHC-DC motion lags BM when measured from a purely transverse angle but leads BM when the measurement axis has a large longitudinal component.

Another oddity in the phase response of OHC-DC is sometimes seen in the base of the gerbil when the beam axis has significant components in the longitudinal and transverse directions — the OHC-DC phase will sometimes exhibit a rapid shift of about a half-cycle. This phenomenon, seen in several experiments from our group, has been heretofore unexplored.

In this work, we show that both of these phenomena are predicted by a simple model of OHC-DC motion in the longitudinal-transverse plane. In our model, the OHC-DC region moves along a very narrow ellipse in which towards-base motion is nearly in-phase with towards-scala media (SM) motion. In the extreme case, this motion is *lineal* (i.e. lying along a straight line), wherein these two components are *precisely* in-phase.

To further validate the model, we also provide longitudinal and transverse components of motion measured in the base of three gerbils *in vivo* at moderately high SPLs. These measurements are achieved using the method of Frost et al. (2023c), which involves measuring from the same position from multiple angles and performing a back-projection. The measurements show near-lineal behavior as well. The approximate direction of this measured motion is illustrated in Fig. 1 **B**.

The manuscript is structured as follows: We first describe the methods used to obtain uniaxial and two-dimensional displacement measurements *in vivo*, including a summary of the method described in Frost et al. (2023c). We follow with a Theory section, in which we motivate and characterize the lineal motion model of OHC-DC displacement. In our Results section, we present measured *in vivo* transverse and longitudinal OHC-DC displacement responses alongside modeled responses. We also show measured phase responses from the gerbil base that exhibit the rapid phase jump predicted by the model. We conclude with mechanical interpretations of the model results and measured responses.

2. Methods

2.1. Animal preparation

Young adult gerbils of either sex were anesthetized with ketamine and pentobarbital. The gerbil's scalp was removed and the head was glued to a two-axis goniometer. The RWM was made visible by exposing and making a narrow hole in the bulla. A Thorlabs Telesto III OCT system equipped with an LSM03 5x objective lens was used to view the OCC through the RWM. Sound stimuli were delivered through a speaker tube situated in the ear canal of the gerbil, and ear canal pressure was monitored with a Sokolich ultrasonic microphone. Sound stimuli were zwuis tone complexes consisting of 25 frequency components each with a randomized phase between 0 and 2π radians. Cochlear condition was assessed by monitoring distortion product otoacoustic emissions (DPOAEs) in response to swept-tone stimuli, and it was ensured that these responses did not significantly decrease over the course of the experiment. Further details of animal preparation and experimental equipment are provided in Strimbu et al. (2020). Experiments were approved by the Columbia University Institutional Animal Care and Use Committee.

The motion characteristics of two preparations, from uniaxial measurements along an axis with both longitudinal and transverse components, are shown as they exhibit a phase lift predicted by our model. Data from Fallah et al. (2019) exhibiting this phase lift is cited as supporting evidence — the same protocol was used for those experiments.

2.2. Summary of the reconstruction method

Longitudinal and transverse components of motion were determined by applying the method described in Frost et al. (2023c). We present a summary of the method here, leaving details to the prior publication.

1. *Coordinate System Determination* — To begin, we orient the system by eye so that our beam axis is perpendicular to the radial axis of the OCC (see Fig. 1 for coordinate axis definitions). We then perform a planar approximation of the BM within the region of the OCC that is visible through the RWM using the

program described in Frost et al. (2022). This gives us a representation of our measurement axis in anatomical coordinates. We ensure that the radial component of the measurement axis is at least ten times smaller than the other two components, so that we can reasonably consider our displacement measurements as projections of only the longitudinal and transverse components of motion.

2. *Measurements of OHC-DC at Many Longitudinal Locations* — We use known anatomy to select a single point at the OHC-DC within a B-Scan. Fig. 2 shows an example of selected points at two different angles. In a B-Scan across the width of the OCC, as in panels **A** and **C**, structures can be recognized by comparison to a standard anatomical cross-section. In the transverse-longitudinal plane (panels **B** and **D**), the BM and OHC-DC regions are separated by a narrow dark band, which must correspond to the fluid-filled tunnels surrounding the outer pillar cells. Use of B-Scans in both of these planes allows us to be confident we are selecting a point at OHC-DC.
   As we know the longitudinal direction from Step 1, we can measure at many positions along a longitudinal line segment (usually between 100 and 150 μm in length, with measured positions spaced 10 μm apart) containing this point. By construction, each measurement line contains both a point on the BM and a point at OHC-DC.
3. *Aligning BM and OHC-DC* — As a result of skew, the OHC-DC and BM points in each A-scan lie in a different longitudinal cross-section. As we know the relationship between anatomical and optical coordinates from Step 1, for each OHC-DC point measured we can determine which BM point lies in the same (or nearly the same) longitudinal cross-section. As such, we can come up with a list of OHC-DC and BM points in the same longitudinal cross-sections as one-another.
4. *Rotate and Repeat* — We rotate the head of the gerbil using a two-axis goniometer so that the beam has a different longitudinal-transverse angle and some of the region measured in Step 2 is still visible. We then repeat Steps 1-3 at this second angle.
5. *Physiology-Based Registration* — Once the experiment has concluded, we observe the BM phase responses from both sets of measurements. We assume that the BM moves purely transversely, so that the phase response of the BM at the same longitudinal position will be the same independent of viewing angle. As such, if we find that the phase response of BM points measured at the two different orientations are the same, then we know the two measurements were made at the same longitudinal position — i.e. the BM points are registered between the angles. OHC-DC points are then registered for free, as they were aligned to BM points in Step 3.
6. *Backprojection* — Each 1-D measurement is a projection of the longitudinal-transverse 2-D motion onto the beam axis (as we have taken care to ensure no radial motion is measured in step 2). We know the beam axes from Step 1, and we have two 1-D measurements, and we want the longitudinal and transverse components that would create such projections. This is a system of two equations in two unknowns and is easily solved by inverting the projection matrix (backprojecting).

The reconstruction analysis was only possible in a few preparations, due to the difficulty to achieve two substantially different angles of measurement, and to signal-to-noise ratio limitations, which are compounded by the reconstruction (Frost et al., 2023c). The results are limited to moderately high-level stimuli (70 and 80 dB SPL) where the signal is sufficiently large to achieve reconstructed motion measurements above the noise floor.

Reconstructions were achieved in three preparations (all shown here), and all supported the main argument of this work: that the OHC-DC region displacement response is near-lineal in the longitudinal-transverse plane with towards-base and towards-SM motion being nearly in phase.

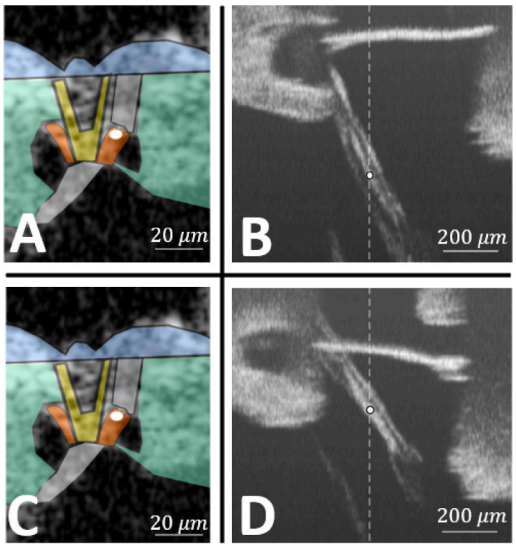

Fig. 2. Examples of B-Scans at various angles from a reconstruction experiment (Ge967). **A** – B-Scan across the width of the organ of Corti, in which structures are color-coded according to known anatomy. One measured position, which we deem to be at OHC-DC, is shown as a white circle. **B** – B-Scan in the longitudinal-transverse plane, orthogonal to that of **A**. The point at OHC-DC is again labeled. **C, D** – The same as **A** and **B** but at a second angle. Panels **A** and **C** are adapted from Frost et al. (2023c). (Note – a reflection of the RWM appears in panels **B** and **D** nearer to the OCC than the RWM actually is. This phenomenon occurs in OCT if an element is too close to the lens. This has no impact on vibrometry within the OCC, which is situated close to the focal distance of the lens.).

For reference, the angles of measurement and noise metrics achieved in each preparation are provided in Table 1. The angles θ_1 and θ_2 are the angles the optic axis made with the BM normal at the first and second measurement orientations, respectively. In all cases, the beam points towards the apex and measurements are made near the 24 kHz region.

The noise multiplier is the factor by which the noise level is increased relative to the uniaxial data, which was derived in Frost et al. (2023c) to be $|\cot\frac{\theta_2-\theta_1}{2}|$.

In uniaxial data, we determine a signal threshold at each measured position, stimulus frequency and stimulus level by finding the mean and standard deviation of the noise in the ten surrounding frequency bins. A signal is considered significant if the measured displacement is more than two standard deviations above the noise floor. We then multiply this threshold value by the noise multiplier to achieve the corresponding threshold for reconstructed data. In Table 1, we present this threshold averaged across frequency and stimulus level at positions from which data is measured as a means of presenting the noise floor as a single number. In practice, the threshold is different at each position/frequency/SPL combination, with the main contributing factor being the reflectivity of the sample at each position (Lin et al., 2017).

2.3. Computer software

Data acquisition software was written in C++, making use of functions from the ThorLabs SpectralRadar SDK. Volume scans used for determining coordinate relationships were acquired using the ThorImage software. Programs for coordinate determination (Frost et al., 2022), reconstruction of 2-D motion (Frost et al., 2023c) and model evaluation were written in MATLAB.

3. Theory

Table 1
Quantitative features of measurements from which reconstructed data is presented in this work. The animal identifier is also presented in each figure containing relevant data.

Animal identifier	θ_1	θ_2	Noise multiplier	Mean signal threshold
Ge967	63°	50°	8.8	1.8 nm
Ge995	45°	59°	8.1	1.6 nm
Ge1013	55°	65°	11.4	2.3 nm

3.1. Review of literature and model motivation

It has long been known or suspected that there are considerable components of intra-OCC displacement in each of the longitudinal, radial and transverse directions. Historically, we have known of significant transverse motion of the organ of Corti through studies of BM displacement (Von Békésy and Wever, 1960; Robles and Ruggero, 2001). The existence of OHC electromotility also implies intra-organ motion in the direction along the cell's length (Frank et al., 1999); this direction is primarily radial and transverse. Fluid mechanics suggests that there should also be a considerable component of longitudinal motion *near* the organ of Corti (and perhaps within it, depending on the impedance of the cells), even in a passive or dead cochlea (Lighthill, 1981, 1978; Steele and Taber, 1979; Frost, 2024). This component of motion is also likely amplified by electromotility — for example, Karavataki and Mountain observed fluid-driven longitudinal motion of tunnel-crossing nerve fibers upon electrical stimulation in an *in vitro* cochlear preparation (Karavataki and Mountain, 2007).

Before the advent of OCT, the relative sizes and phases of these components of intra-OCC motion were not known. Displacement responses measured via OCT have confirmed the existence of large intra-organ displacement responses, and the technology has also allowed us to compare simultaneous responses at different positions in the OCC. However, the limitations of OCT discussed in the Introduction, particularly those involving ambiguities in measured phase responses, have made it challenging to synthesize data from various experimental preparations (Olson et al., 2025). We aim to tackle this synthesis through a model informed by OCT-measured displacement responses, *in vivo* in gerbil, with a specific focus on motion in the longitudinal-transverse plane. We first review these data as motivation for our model.

Cooper et al. were among the first to measure OCC micromechanics in the gerbil base *in vivo* using OCT (Cooper et al., 2018). The majority of their data was recorded with a beam axis with components in all three anatomical directions, with the longitudinal component being positive — that is, the beam is pointed towards the apex. The displacement responses shown in their Fig. 7 show a broadband phase lead of OHC-DC relative to BM. This same phase lead is seen by Frost et al. after correcting for skew in a similar preparation (Frost et al., 2022, 2023c), and by Meenderink and Dong at a more apical location (Meenderink and Dong, 2022).

It is anatomically challenging to achieve displacement responses through the gerbil RWM with the optical axis having a negative longitudinal component — that is, with the beam pointing towards the base. Cooper et al. achieved such measurements in two preparations, and found a broadband *lag* of OHC-DC relative to BM (seen in their Fig 8).

Meenderink and Dong observed OHC motion at various positions along the longitudinal axis of the gerbil cochlea (~3 kHz region) without changing the beam angle, so that at each point of measurement the beam axis had a different longitudinal component (Meenderink and Dong, 2022). They found that between apical-pointing and basal-pointing angles, there was a rapid phase shift of half of a cycle, with (again) the OHC region leading BM at apical-pointing angles and lagging BM at basal-pointing angles. The authors found that this rapid shift occurred close to the point at which the beam was purely transverse-radial, which they interpreted as a dominance of longitudinal motion at the OHC region. However, their measurement axes contained large radial and transverse components — in fact, from their B-Scan in their Fig. 1, it appears that their measurement axis was perpendicular to the length of the OHC. As such, the data imply that longitudinal axis was dominant over the motion orthogonal to the OHC in a given longitudinal cross-section. While this is an important result, it is not easily interpreted in terms of the function of the outer hair cells whose motion *along their length*, i.e. perpendicular to Meenderink's and Dong's beam axis, is expected to be critical for cochlear function.

Near-purely transverse motion measurements – that is, the longitudinal component of the beam is ~ 0 – have been achieved through the gerbil RWM (Cho and Puria, 2022; Strimbu and Olson, 2022; Strimbu et al., 2024), and show significant motion at the OHC-DC (if the motion were greatly dominated by the longitudinal component in this plane, one would expect a very small magnitude of displacement at this purely transverse angle). In purely transverse data, a broadband *lag* of OHC-DC relative to BM is seen, as in the measurements from basal-pointing angles described above.

Lastly, in Frost et al. (2023c) we presented a method for measuring longitudinal and transverse displacement responses and showed preliminary data from a single preparation (~25 kHz place through gerbil RWM). We saw that longitudinal and transverse motion at OHC-DC were similar in magnitude, and that towards-base and towards-SM motion were approximately in-phase at the moderately high SPLs reported. We have since seen similar results in two other preparations, displayed in the Results section.

Together, these data point to significant longitudinal and transverse components of motion that are *out of phase* from one another with the axes' directions as noted in Fig. 1. This would suggest the presence of a destructive interference between the longitudinal and transverse components of motion when they are projected along a towards-apex optical axis, as opposed to a constructive interference when they are projected along a towards-base beam.

As a result, varying the angle of measurement in the longitudinal-transverse plane (with a towards-apex optical axis) should result in a rapid jump in phase at a particular angle. The angle at which this jump occurs would likely be frequency- and SPL-dependent, and thus the jump might also be observed at a fixed angle of measurement, while varying frequency. We have observed relevant phase jumps in some displacement data from the gerbil base, for example Fig. 6 of Fallah et al. (2019). We show more such examples in the Results section.

All of these results suggest that motion at the OHC-DC is nearly lineal – that is, along a straight line – in the longitudinal-transverse plane, with towards-base and towards-SM motion being nearly in-phase as shown in Fig. 1 **B**. We are thus motivated to explore a simple model in which the motion at the OHC-DC region is precisely lineal with these relative phases.

3.2. Lineal motion model

Say $\mathbf{d}^o(f) = (d_l^o(f) \quad d_t^o(f))^T \in \mathbb{C}^2$ is the true OHC-DC motion written in its longitudinal and transverse components (again, we have set our measurement axes so that we measure no radial motion), where f is stimulus frequency. Say the beam axis makes an angle θ with the BM normal. Writing the components in polar form (where $\angle$ denotes the phase of the complex number and j is the imaginary unit), the measured motion at the OHC-DC is

$$\delta^o(f,\theta) = |d_l^o(f)|e^{j\angle d_l^o(f)} \sin\theta + |d_t^o(f)|e^{j\angle d_t^o(f)} \cos\theta. \quad (1)$$

Assuming the two components are precisely a half-cycle out of phase, we have

$$e^{j\angle d_l^o(f)} = e^{j(\pi+\angle d_l^o(f))} = -e^{j\angle d_l^o(f)}, \tag{2}$$

$$\delta^o(f,\theta) = (|d_l^o(f)|\sin\theta - |d_t^o(f)|\cos\theta)e^{j\angle d_l^o(f)}. \tag{3}$$

Considering the cases where the leading term is either positive or negative gives the formulae for magnitude and phase of measured OHC-DC displacement in the lineal motion model:

$$|\delta^o(f,\theta)| = \left||d_l^o(f)|\sin\theta - |d_t^o(f)|\cos\theta\right|, \tag{4}$$

$$\angle\delta^o(f,\theta) = \begin{cases} \angle d_l^o(f), & |d_l^o(f)|\sin\theta > |d_t^o(f)|\cos\theta \\ \angle d_t^o(f) = \angle d_l^o(f) + \pi, & |d_l^o(f)|\sin\theta < |d_t^o(f)|\cos\theta. \end{cases} \tag{5}$$

Notably, the phase response exhibits a "winner-takes-all" behavior, where the measured phase is that of the largest projected component — that is, for each frequency-angle combination, one measures the phase response of either the longitudinal or transverse component. The responses in Fig. 3 show that the components have comparable magnitudes across frequency. This means that for relatively small or large viewing angles, one should expect the uniaxially measured phase response to precisely match that of the transverse or longitudinal component, respectively.

4. Results

The Results section comprises three subsections — we first present measured longitudinal and transverse components of motion that show further evidence for lineal motion in the OHC-DC region (Figs. 3 and 4). We then show examples of the phase lifts seen in mixed-angle preparations that we predict as a consequence of the lineal model (Fig. 5). These serve as supporting data for the model. We lastly show results of the lineal model in comparison to these data.

4.1. Longitudinal and transverse components of motion

Fig. 3 shows longitudinal and transverse gain amplitude responses from the OHC-DC region in three preparations (see Table 1 for details on angles of measurement). Notable features: the longitudinal and transverse components have comparable amplitudes to one another at both tested SPLs; for both components of motion, responses at 70 dB SPL have larger gains than those at 80 dB SPL across the measured frequency range, i.e. transverse and longitudinal components both display broadband nonlinearity. Broadband nonlinearity is characteristic of OHC-DC displacement responses when multi-tone stimuli are used, where it emerges at moderate (individual-tone) SPL because the overall sound level is substantially higher than the level of the individual tones (Cooper et al., 2018; Strimbu et al., 2018; Strimbu and Olson, 2022; Strimbu et al., 2024). When single-tone stimuli are used, broadband nonlinearity can emerge at high SPL (Cho and Puria, 2022; Strimbu and Olson, 2025).

Fig. 4 shows longitudinal and transverse phase responses at the BM and OHC-DC at two distinct longitudinal locations for each preparation. Also displayed are the transverse phase responses shifted vertically by 0.5 cycles. In this shifted form they represent transverse motion towards scala tympani. Notable features: the longitudinal and transverse components are out of phase by approximately a half-cycle across frequency (the half-cycle-shifted transverse phase and the longitudinal phase lie nearly on top of one another); longitudinal phase leads BM while transverse phase lags BM across frequency in most cases. In Ge967, the transverse phase meets the BM phase near the BF — a feature seen in some near-purely transverse measurements at high levels (Strimbu et al., 2024).

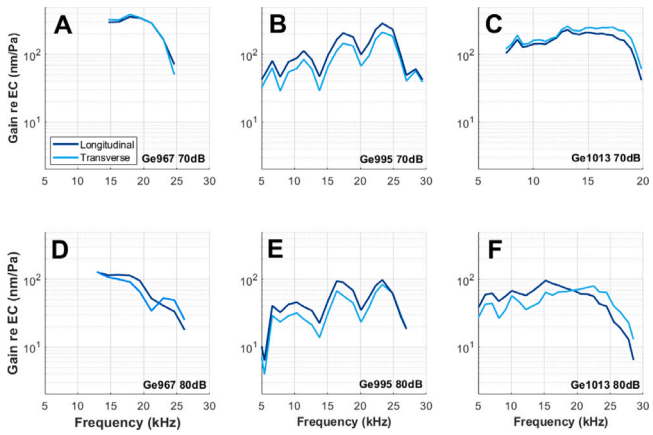

Fig. 3. Longitudinal and transverse components of OHC-DC displacement gain magnitude relative to ear canal (EC) pressure in response to 70 dB SPL (**A-C**) and 80 dB SPL (**D-F**) zwuis tone complexes, measured through the RWM of gerbil in three different preparations.

4.2. Phase lifts in uniaxial measurements

Fig. 5 shows OHC-DC responses measured through the RWM along a beam axis containing significant components in both the longitudinal and transverse directions, at 60 and 80 dB SPL. Measurement angles were not precisely determined in these experiments, but we expect the angle to be comparable to those seen in Table 1 ($\sim 45°$ to $65°$ with the BM normal) as the same method was used to achieve a view of the OCC in each of these experiments.

Five responses are shown from within the OHC-DC regions of two preparations. In all five phase response plots (**F-J**), a rapid and persistent lift is seen in the 80 dB phase response at a frequency near the BF, but is not seen in the 60 dB phase responses. The differences between the higher- and lower-level phase responses are shown in panels **K-O**. The difference value is seen to rapidly approach about one half-cycle. Near the lift frequency, the high-level magnitude responses display local minima (panels **A**, **C-E**), or an inflection point (panel **B**). Multiple responses from each animal are presented to indicate that these features of the data are robust in preparations in which they occur.

4.3. Model results

4.3.1. Consequences of pure lineal motion for uniaxial measurements

The data in Section 4.1 show that the displacement responses at OHC-DC in response to high-level stimuli follow a near-lineal pattern across frequency, with towards-SM motion close to a half-cycle out of phase with towards-apex motion. This motivates the model described in Section 3.2. The model is useful in describing certain features of uniaxially measured data such as the phase lifts shown in Section 4.2, as it exhibits a discontinuous phase response according to Eq. (5).

As the ratio of the components' magnitudes varies in frequency, at viewing angles where the beam axis has significant components in both anatomical directions the "winner" of Eq. (5) may change across frequency. For a given viewing angle θ, there may exist one or more frequencies $f_\perp$ at which the dominant projected component changes. This would correspond to a phase shift of a half-cycle seen in the frequency response at $f_\perp$. For ideal lineal motion as described in Eqs. (4) and (5), this phase shift would be instantaneous, and would correspond to a null in the magnitude response at $f_\perp$.

This concept is illustrated in Fig. 6, which shows the projection of lineal motion onto the OCT beam in three cases. In panel **A**, longitudinal motion dominates the projection, and the measured displacement phase will match that of the longitudinal component (the first case

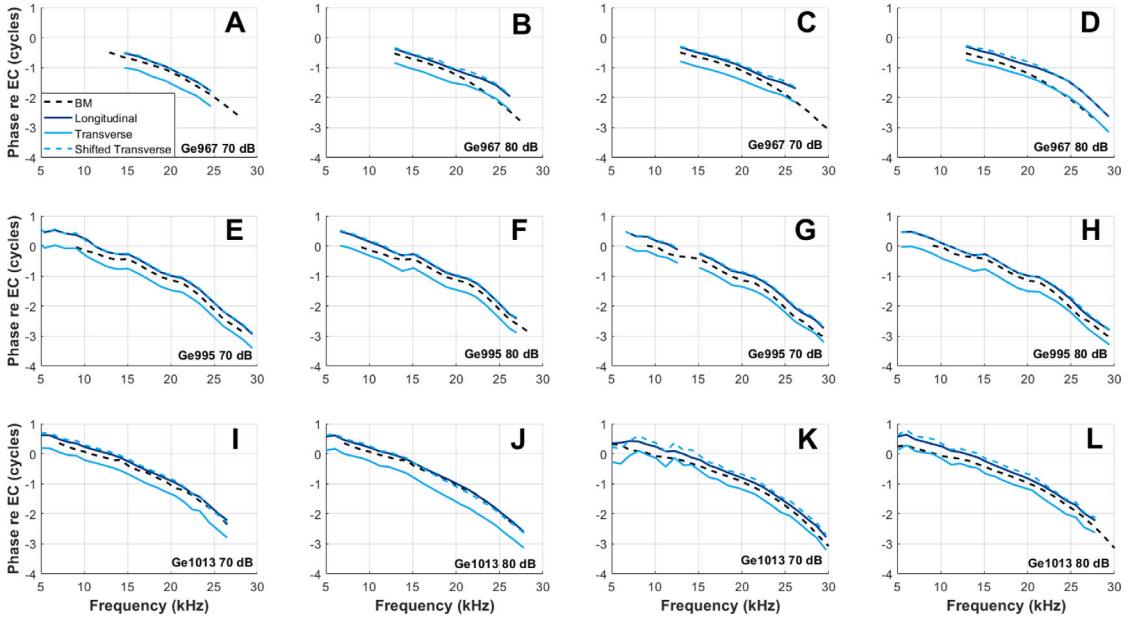

Fig. 4. Longitudinal and transverse components of OHC-DC displacement phase relative to ear canal (EC) pressure in response to 70 dB SPL and 80 dB SPL zwuis tone complexes, measured through the RWM of gerbil in three different preparations. "Shifted Transverse" responses are the transverse responses shifted vertically by 0.5 cycles. **A, B**: 70 and 80 dB SPL responses at one longitudinal position in Ge967. **C, D**: Same as **A** and **B**, but measured at a distinct longitudinal location 20 μm apical of the first set. **E-H**: Same as **A-D**, but in Ge995. Second set measured 30 μm apical of first set. **I-L**: Same as **A-D**, but in Ge1013. Second set measured 30 μm apical of first set. BM displacement was found at the same longitudinal locations of OHC-DC in each panel; BM phase is shown in the black dashed lines.

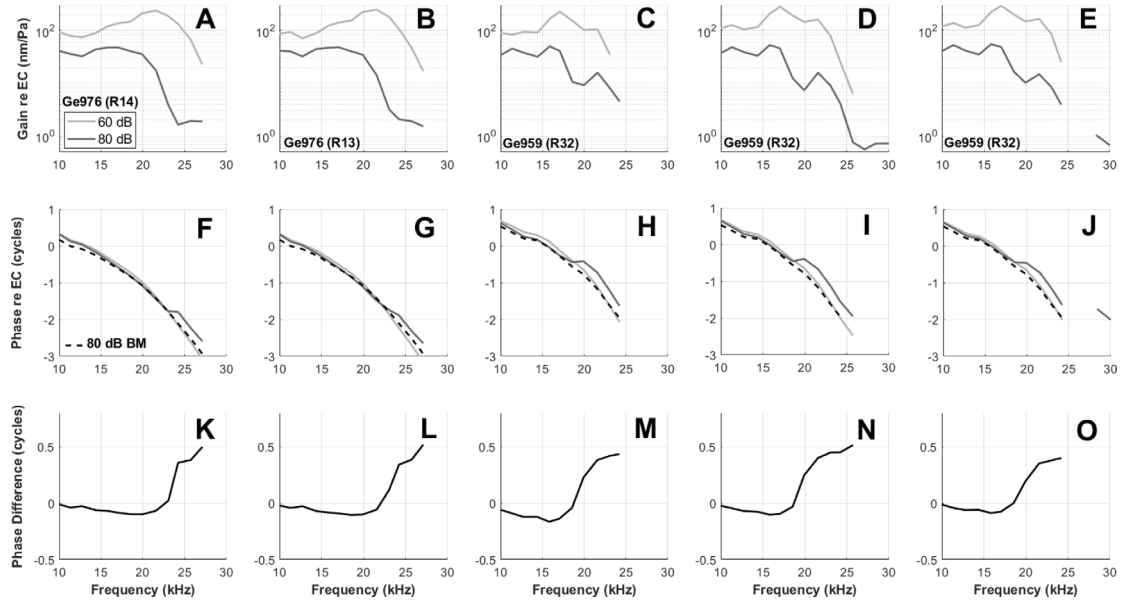

Fig. 5. **A, B**: OHC-DC displacement gain magnitude relative to ear canal (EC) pressure in response to 60 dB SPL and 80 dB SPL zwuis tone complexes, measured through the RWM of Ge976. The measurement axis had components in both the longitudinal and transverse directions. **C-E**: Same as **A, B** but in Ge959. Different columns correspond to distinct locations within the OHC-DC region of the cochlea. Distinct run numbers (which appear in parentheses) correspond to measurements at distinct longitudinal positions within the cochlea. **F-J**: Phase responses corresponding to **A-E**, each showing distinct phase lifts in the higher-level response. BM phase is included as a dashed line for completeness and comparison to previous data; in this figure due to skew BM motion is measured in a cross-section ~ 50 μm basal to measured OHC-DC. **K-O**: The difference between the higher-level and lower-level phase responses from panels **F-J**. Data from **D, I** were previously presented in Strimbu et al. (2024).

of Eq. (5)). In **B**, the line segment of motion is precisely perpendicular to the beam axis (i.e. this is the response at $f_{\perp}$), and no motion will be measured. In **C**, transverse motion dominates the projection, and the measured displacement phase will match that of the transverse component (the second case of Eq. (5)). Note that in **A** the projection is along the negative beam axis while in **C** the projection is onto the positive beam axis, in accord with the expected half-cycle shift.

4.3.2. *Phase lifts arising from lineal and near-lineal motion patterns*

The phase relation of Eq. (5) suggests the possibility of a phase lift of the character seen in the uniaxially measured data of Fig. 5. Fig. 7 **A-D** shows a simulated ideal lineal displacement response in which this phase lift would occur. The longitudinal and transverse components have constant phase of 0 and −0.5 cycles respectively, the longitudinal displacement magnitude is constant and the transverse displacement magnitude increases in frequency.

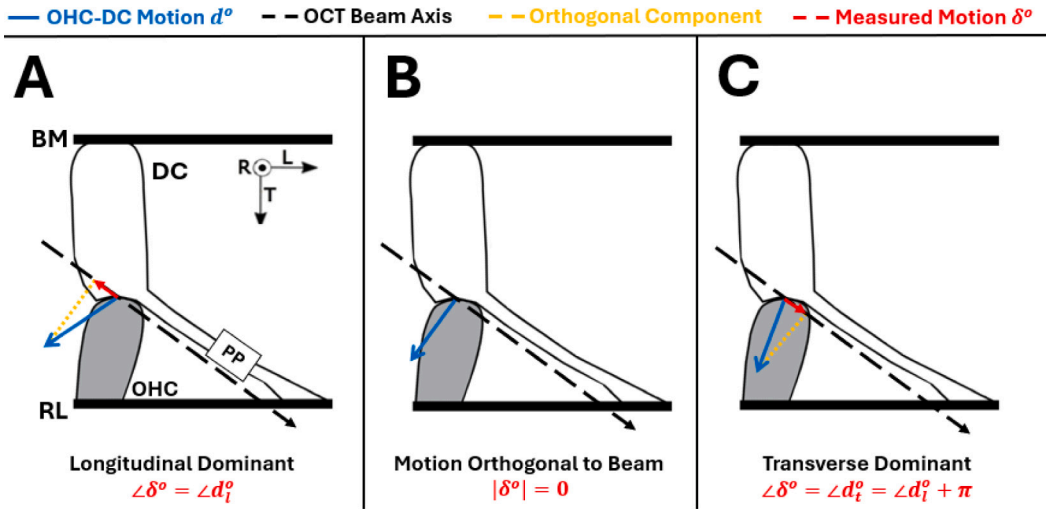

Fig. 6. Illustration of the theoretical impact of ideal lineal motion on uniaxially measured OHC-DC gain responses. **A** – The longitudinal component of motion is dominant along the beam axis, so measured motion would be in phase with the longitudinal component. **B** – The beam axis is perpendicular to the line of motion, so no motion is measured. **C** – The transverse component of motion is dominant along the beam axis, so measured motion would be in phase with the transverse component (precisely 0.5 cycles out of phase with the longitudinal component).

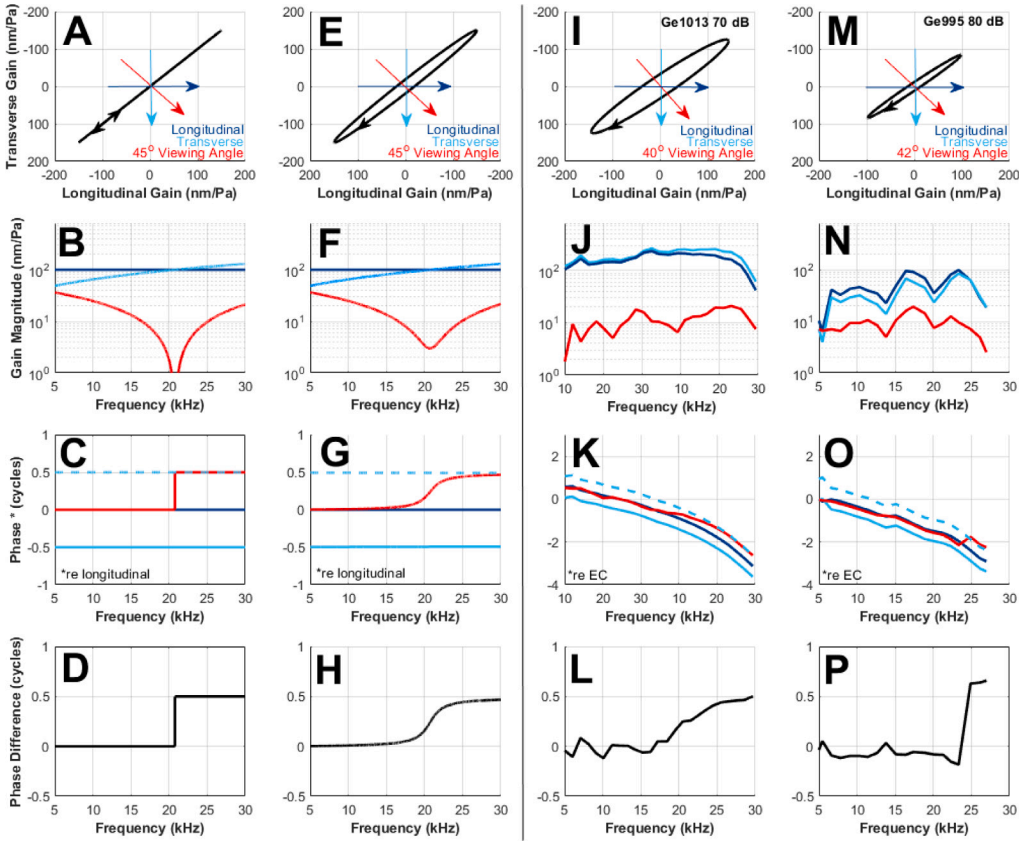

Fig. 7. Illustration of the source of phase lifts of the type seen in Fig. 5 using simulated and measured OHC-DC responses at three viewing angles. **A**: A simulated line of motion in the longitudinal-transverse plane, where the components are precisely half-a-cycle out of phase. **B, C**: Gain magnitude and phase responses of simulated ideal lineal motion viewed from three angles — a longitudinal angle, a transverse angle and a 45° angle with the transverse axis. Phase is presented in cycles relative to the phase of the simulated longitudinal component. The longitudinal component was set to have constant magnitude and phase, and the transverse component was made to slowly increase in magnitude, also with a constant phase (−0.5 cycles out of phase with the longitudinal component). The dashed line in the phase plot shows transverse displacement shifted up by one cycle. Displayed line of motion in **A** shows the response near the point at which the transverse and longitudinal component are equal in magnitude. **D**: Difference between phase measured at the mixed angle and longitudinal phase. **E-H**: Same as **A-D**, but for simulated near-lineal motion where transverse motion lags elliptical motion by 0.52 cycles across frequency. Motion pattern in **E** shows the response near the middle of the phase lift region. **I-L**: Same as **A-D**, but using measured longitudinal and transverse motion from Ge1013, and those components projecting onto an axis making a 40° angle with the transverse axis. The shown ellipse in **I** is the response at 20 kHz, where the components are 0.525 cycles out of phase. The phase responses in panel **K** are relative to ear canal (EC) pressure. **M-P**: Same as **I-L**, but in Ge995 using a 42° mixed angle. The shown ellipse in **M** is the response at 23 kHz where the components are 0.522 cycles out of phase.

Responses are shown projected onto a beam with a viewing angle 45° from the transverse axis. At lower frequencies, the measured phase matches the longitudinal phase precisely, as this is the component dominant in the projection. At the frequency where the two components of motion are equal, $f_{\perp}$, the magnitude drops to 0 and the phase discontinuously jumps by 0.5 cycles to be in phase with transverse motion, in accord with Eqs. (4) and (5). (We select 45° as the simulated viewing angle somewhat arbitrarily — if we had chosen a different angle, the phase jump/amplitude notch would still occur but at a different frequency.)

Such discontinuities are not actually seen in data where phase lifts are present — in Fig. 5, it is seen that the lifts are rapid but not instantaneous and that the gain magnitude does not dip to 0. This indicates that measured motion is not precisely lineal. On the other hand, reconstructions of longitudinal-transverse components show that phase differences between longitudinal and transverse components are very nearly 0.5 cycles across frequency (see Fig. 4), indicating that the responses are very nearly lineal. This is explained by the fact that even a small deviation from lineal motion can yield a gentler magnitude trough and phase lift than what is seen in the ideal lineal case. Fig. 7 **E-H** show a simulated near-lineal response, identical to that of **A-D** save that the phases now differ by 0.52 cycles across frequency rather than exactly 0.5 cycle. This results in the narrow elliptical motion pattern seen in panel **E**. The magnitude trough and phase lift are still present, but occur over a broader frequency range — that is, there is no precise $f_{\perp}$. The simulated phase difference seen in panel **H** resembles more closely the phase lifts seen in the uniaxially measured data of Fig. 5.

Fig. 7 **I-P** show longitudinal and transverse displacement responses measured in gerbil along with their projections onto hypothetical beam axes with significant components in both the longitudinal and transverse directions. This synthetic projection yields a phase lift – more gentle in **I-L** and more rapid in **M-P** – resembling the uniaxially measured data of Fig. 5. Near the frequency at which this lift occurs, we plot the ellipses of motion (**I** and **M**) and see that they are narrow but not precisely lineal. At this frequency, the difference between longitudinal and transverse phase is 0.525 for Ge1013 and 0.522 for Ge995, indicating the significance of small deviations from perfect lineality. Notable also is the relatively low magnitude of the projected motion. This is due to the projections of the two out-of-phase components "subtracting" with one another (as they are approximately one half-cycle out of phase, see Eq. (4)), which corresponds to the near-perpendicularity of the beam axis and the line of motion (see Fig. 6 **B**).

It should be noted that the phase differences presented in Figs. 5 and 7 are different objects — the former is a difference between high- and low-level responses, and the latter is a difference between a simulated mixed-angle-measured response and the longitudinal response. Within the near-lineal motion framework, the displayed lower-level phase responses in Fig. 5 (in which no lifts occur) are approximately equal to the longitudinal phase response, so the two ways phase difference was plotted in Figs. 5 and 7 are comparable. This is validated by the similarity between the phase differences in the two figures.

Related to the above, although the mechanism for the phase lift is not overtly SPL-dependent, we have only seen it appear at high SPL (e.g. 80 dB responses in Fig. 5). This suggests that at lower SPL the longitudinal component of motion is larger relative to transverse than it is at higher SPL. In that case, if measurements were made at an angle slightly more transverse than longitudinal, a phase lift would be predicted to be observable at lower SPL. Such an observation would reinforce the lineal motion finding of this report, and extend the finding to lower SPL.

In published data from the gerbil base, the phase lifts observed in Fig. 5 are quite rare. This indicates that the viewing angle is typically sufficiently longitudinal or transverse that the dominant projected component never switches. As the relative gains of the transverse and longitudinal components are similar across frequency, and their ratio does not appear to vary rapidly (Fig. 3), a viewing angle of about 45° is required to see the lift (as simulated in Fig. 7). This explains the stark difference between the OHC-DC – BM phase responses measured in the ~ 45 kHz hook region (a primarily transverse viewing angle) and those measured near the 25 kHz place (a primarily longitudinal angle), as each viewing angle is sufficiently extreme to yield near-completely transverse or longitudinal OHC-DC phase responses, respectively (Frost et al., 2023c; Strimbu et al., 2024).

It is important to distinguish the phase lift observed in Figs. 5 and 7 from a phase lift of different cause that is sometimes seen in OHC-DC motion responses measured with a relatively transverse angle. For example, Strimbu et al. observed that in the gerbil hook region, high-level OHC-DC responses can exhibit a phase lift at a frequency below/above which OHC-DC and BM move out-of-phase/in-phase (Strimbu et al., 2024). The authors argued that this phase lift is due to a dominance trade-off between active internal OHC motion and BM motion. This type of phase lift can be seen in the transverse phase responses in Fig. 4 **B**.

5. Discussion

Our data show that, at least in response to moderately high-level stimuli, transverse and longitudinal components of motion at the OHC-DC are similar in magnitude and are both nonlinear across frequency (Fig. 3). Broadband nonlinearity in response to multi-tone stimuli is characteristic of the region of the organ of Corti near OHC-DC, and is not generally present at the BM, reticular lamina (RL), or in the lateral supporting cells (irrespective of viewing angle) (Strimbu et al., 2024; Cooper et al., 2018). This leads one to believe that longitudinal OHC-DC motion is driven by active OHC forces (e.g. electromotility). This expectation is bolstered by the fact that in response to electrical stimulation, OHC-driven longitudinal motion of tunnel-crossing nerve fibers was visualized in an *in vitro* cochlea preparation (Karavataki and Mountain, 2007).

While OHCs themselves are longitudinally slanted in some species, this is not particularly pronounced in the base of gerbil (Yoon et al., 2011), so OHC-driven longitudinal motion is not arising directly from an electromotile push in this direction. Instead, it may come from interaction with the longitudinally-processing cytoarchitecture of the organ of Corti.

As seen in Fig. 1 **B**, DCs connect to RL through longitudinally-slanting microtubule-packed phallangeal processes (PP), and connect to the BM through the Deiters' stalk (Parsa et al., 2012). As OHCs expand and contract, pushing on DC within the same longitudinal cross-section, the phallangeal processes of the DC will also move and push on RL at a more apical cross-section. This is one mechanism by which OHC-driven longitudinal motion might arise, and may even be used to sharpen/amplify the traveling wave.

Considering the effects of electromotility only, lineal motion makes sense — a push from OHCs at DC would result in the PP, now being pulled towards BM, to hinge towards the apex to maintain their length. Thus, at OHC-DC we would see a towards-BM, towards-apex *lineal* motion. This is precisely the vector of motion seen in our results.

Of course, in the real cochlea there are far more factors than electromotility, and one would not expect the above argument to hold across stimulus level and frequency. However, it does provide some mechanical intuition as to the forces at play that may lead to near-lineal motion.

Having considered the origin of this motion, it is then natural to ask: what is its use, if any? The above argument is suggestive of a potential feedforward mechanism in the organ of Corti — one in which OHC action at one cross-section leads to forces at more apical cross-sections. Cochlear models at various levels of abstraction have shown that feedforward mechanisms could sharpen the tuning of the traveling wave (Yoon et al., 2011; Motallebzadeh et al., 2018; Guinan, Jr., 2022). Most relevant to this study is the work of Motallebzadeh et al. (2018), in which an active cochlear model containing the PP was implemented.

The authors compared this model to ones in which the PP were either not present or oriented in the opposite direction. They found that properly oriented PP enhanced both the amplitude and sharpness of tuning of the traveling wave.

It has also been argued by Guinan that longitudinal coupling through intra-organ fluid, along with push/pull mechanisms through the PP, are responsible for amplification of the traveling wave (Guinan, Jr., 2022). His "area pump" model similarly relies on lineal motion of OHC-DC to achieve conservation of volume as the cross-sectional area of the OCC expands and contracts simultaneously in different cross-sections.

Other modelers have argued *against* the criticality of longitudinal feedforward mechanisms, and propose instead models in which local amplification is dominant (de Boer, 2007; Shera and Altoè, 2023). The results presented in this work do not inherently undercut such models — it is not necessarily the case that this lineal motion does useful mechanical work at all points basal to the best place. Given the majority of the OCC is isolated from the nonlinear boosting of OHC-DC motion (in both longitudinal and transverse directions) except for at frequencies close to the BF (Strimbu et al., 2024), it may be the case that the transverse-longitudinal action of the OHCs is not globally feedforward but only has a small range in which it meaningfully contributes to amplification.

6. Conclusions and future work

In the present work, we have provided evidence of narrow elliptical (near-lineal) OHC-DC motion patterns in the longitudinal-transverse plane in the gerbil base at moderately high SPL. The data reveal a cause of phase response oddities in some uniaxial measurements, broadband nonlinearity in the longitudinal component of motion, and motion in the longitudinal-transverse plane in very narrow ellipses. These results raise further questions about the significance of longitudinal motion in the OCC.

We have shown that there is some active contribution to the longitudinal component of motion, as the responses are nonlinear across frequency, but it may also be enlightening to probe the passive OHC-DC response. In a passive cochlea, longitudinal motion may still arise from the architecture of the OCC and the need to conserve intra-OCC fluid volume in the presence of a traveling wave. Conversely, it is important to probe similar questions at lower stimulus levels *in vivo*, where nonlinearity and the impact of OHC activity are more pronounced.

Another natural question is whether or not the other cell groups in the OCC move in lineal patterns as well. While the cells lateral of the OHCs, such as the tectal or Hensen's cells, may not be mechanically imperative, their behavior could provide insight into more global properties of the OCC. These cells may simply behave like the fluid near the organ of Corti, in which case one would expect non-degenerate elliptical displacement responses.

Our inability to achieve either *post mortem* data or data at lower SPLs is caused by the hours-long data collection time (over which a dead cochlea will degrade) and the noise increase caused by the reconstruction method. This same time limitation has made it challenging to measure 3-D motion – longitudinal, radial and transverse components — in a single sample. While radial-transverse reconstructions in mouse have been published (Lee et al., 2016), it would be interesting to see how these results appear in gerbil base alongside longitudinal motion patterns.

The displacement responses of the lateral cells are measurable with OCT, but their relatively low reflectivity in gerbil makes the signal-noise-ratio of displacement responses in this region lower than those at OHC-DC. This reduces the efficacy of our reconstruction method at these locations.

Advances in the method may allow for these roadblocks to be overcome, for example, through the use of the compressed sensing vibrometry technique, which accelerates acquisition of OCT displacement data (Frost et al., 2023a).

Alternatively, certain features could be probed without reconstruction. For example, one could observe phase responses relative to BM in the lateral region or OHC-DC region when the beam axis is pointed apically vs. basally, and observe characteristic differences (similar to Cooper et al. (2018), or Meenderink and Dong (2022)) that may reinforce or preclude the presence of near-lineal motion at a given location.

CRediT authorship contribution statement

Brian L. Frost: Writing – original draft, Software, Methodology, Investigation, Funding acquisition, Formal analysis, Conceptualization. **C. Elliott Strimbu:** Writing – review & editing, Software, Methodology, Formal analysis, Data curation, Conceptualization. **Elizabeth S. Olson:** Writing – review & editing, Supervision, Resources, Project administration, Methodology, Investigation, Funding acquisition, Conceptualization.

Funding

Funding was provided by NIDCD grants R01 DC015362 (Elizabeth Olson PI) and F31 DC020621 (Brian Frost PI).

Declaration of competing interest

The authors declare that they have no known competing financial interests or personal relationships that could have appeared to influence the work reported in this paper.

Data availability

Data will be made available on request.

References

Altoè, A., Dewey, J.B., Charaziak, K.K., Oghalai, J.S., Shera, C.A., 2022. Overturning the mechanisms of cochlear amplification via area deformations of the organ of Corti. J. Acoust. Soc. Am. 152 (4), 2227–2239. http://dx.doi.org/10.1121/10.0014794.

Cho, N.H., Puria, S., 2022. Motion of the cochlear reticular lamina implies that it is not a stiff plate. Sci. Rep. 12 (1), 18715.

Cooper, N.P., Vavakou, A., Van Der Heijden, M., 2018. Vibration hotspots reveal longitudinal funneling of sound-evoked motion in the mammalian cochlea. Nat. Commun. 9 (1), 3054. http://dx.doi.org/10.1038/s41467-018-05483-z.

de Boer, E., 2007. Forward and reverse waves in nonclassical models of the cochlea. J. Acoust. Soc. Am. 121 (5), 2819–2821.

Dong, W., Xia, A., Raphael, P.D., Puria, S., Applegate, B.E., Oghalai, J.S., 2018. Organ of Corti vibration within the intact gerbil cochlea measured by volumetric optical coherence tomography and vibrometry. J. Neurophysiol. 120, http://dx.doi.org/10.1152/jn.00702.2017.

Fallah, E., Strimbu, C.E., Olson, E.S., 2019. Nonlinearity and amplification in cochlear responses to single and multi-tone stimuli. Hear. Res. 377, 271–281. http://dx.doi.org/10.1016/j.heares.2019.04.001.

Frank, G., Hemmert, W., Gummer, A.W., 1999. Limiting dynamics of high-frequency electromechanical transduction of outer hair cells. Proc. Natl. Acad. Sci. 96 (8), 4420–4425. http://dx.doi.org/10.1073/pnas.96.8.4420.

Frost, B.L., 2024. Foundations of the WKB approximation for models of cochlear mechanics in 1- and 2-D. Revis. J. Acoust. Soc. Am. 155, 358–379.

Frost, B.L., Janjušević, N., Strimbu, C.E., Hendon, C., 2023a. Compressed sensing of displacement signals measured with optical coherence tomography. Biomed. Opt. Express 14 (11), 5539–5554.

Frost, B.L., Strimbu, C.E., Olson, E.S., 2022. Using volumetric optical coherence tomography to achieve spatially resolved organ of Corti vibration measurements. J. Acoust. Soc. Am. 151, 1115–1125.

Frost, B., Strimbu, C.E., Olson, E.S., 2023b. Erratum: Reconstruction of transverse-longitudinal vibrations in the organ of Corti complex via optical coherence tomography. J. Acoust. Soc. Am. 153, 2537–2538.

Frost, B., Strimbu, C.E., Olson, E.S., 2023c. Reconstruction of transverse-longitudinal vibrations in the organ of Corti complex via optical coherence tomography. J. Acoust. Soc. Am. 153, 1347–1360.

Guinan, Jr., J.J., 2022. Cochlear amplification in the short-wave region by outer hair cells changing organ-of-Corti area to amplify the fluid traveling wave. Hear. Res. 426, 108641.

Karavataki, K.D., Mountain, D.C., 2007. Evidence for outer hair cell driven oscillatory fluid flow in the tunnel of Corti. Biophys. J. 92, 3284–3293.

Lee, H.Y., Raphael, P.D., Xia, A., Kim, J., Grillet, N., Applegate, B.E., Bowden, A.K.E., Oghalai, J.S., 2016. Two-dimensional cochlear micromechanics measured in vivo demonstrate radial tuning within the mouse organ of Corti. J. Neurosci. 36 (31), 8160–8173. http://dx.doi.org/10.1523/jneurosci.1157-16.2016.

Lighthill, J., 1978. Waves in Fluids. Cambridge University Press.

Lighthill, J., 1981. Energy flow in the cochlea. J. Fluid Mech. 106, 149–213. http://dx.doi.org/10.1017/S0022112081001560.

Lin, N.C., Hendon, C.P., Olson, E.S., 2017. Signal competition in optical coherence tomography and its relevance for cochlear vibrometry. J. Acoust. Soc. Am. 141 (1), 395–405. http://dx.doi.org/10.1121/1.4973867.

Meenderink, S., Dong, W., 2022. Organ of Corti vibrations are dominated by longitudinal motion in vivo. Commun. Biol. http://dx.doi.org/10.21203/rs.3.rs-1405408/v1.

Motallebzadeh, H., Soons, J.A.M., Puria, S., 2018. Cochlear amplification and tuning depend on the cellular arrangement within the organ of Corti. PNAS 115 (22), 5762–5767.

Olson, E.S., Dong, W., Applegate, B.E., Charaziak, K.K., Dewey, J.B., Frost, B.L., Meenderink, S.W., Nam, J.-H., Oghalai, J.S., Puria, S., Ren, T., Strimbu, C.E., Van Der Heijden, M., 2025. Visualizing motions within the cochlea's organ of Corti and illuminating cochlear mechanics with optical coherence tomography. Hear. Res. 455, 109154. http://dx.doi.org/10.1016/j.heares.2024.109154.

Parsa, A., Webster, P., Kalinec, F., 2012. Deiters cells tread a narrow path – The Deiters cells-basilar membrane junction. Hear. Res. 290, 13–20.

Pierre, P.V., Rasmussen, J.E., Aski, S.N., Damberg, P., Laurell, G., 2020. High-dose furosemide enhances the magnetic resonance signal of systemic gadolinium in the mammalian cochlea. Otol. Neurotol. 41 (4), 545–553. http://dx.doi.org/10.1097/mao.0000000000002571.

Rabbitt, R.D., 2022. Analysis of outer hair cell electromechanics reveals power delivery at the upper-frequency limits of hearing. J. R. Soc. Interface 19 (191).

Rabbitt, R., Bione, T., 2023. A parametric blueprint for optimum cochlear outer hair cell design. J. R. Soc. Interface 20 (199), 20220762.

Robles, L., Ruggero, M.A., 2001. Mechanics of the mammalian cochlea. Physiol. Rev. 81 (3), 1305–1352. http://dx.doi.org/10.1152/physrev.2001.81.3.1305.

Shera, C.A., Altoè, A., 2023. Otoacoustic emissions reveal the micromechanical role of organ-of-Corti cytoarchitecture in cochlear amplification. Proc. Natl. Acad. Sci. 120 (41).

Steele, C.R., Taber, L.A., 1979. Comparison of WKB and finite difference calculations for a two-dimensional cochlear model. J. Acoust. Soc. Am. 65 (4), 1001–1006. http://dx.doi.org/10.1121/1.382569.

Strimbu, C.E., Chiriboga, L.A., Frost, B.L., Olson, E.S., 2024. Regional differences in cochlear nonlinearity across the basal organ of Corti of gerbil: Regional differences in cochlear nonlinearity. Hear. Res. 443, 108951.

Strimbu, C.E., Lin, N.C., Olson, E.S., 2018. Optical coherence tomography reveals complex motion between the basilar membrane and organ of Corti in the gerbil cochlea. J. Acoust. Soc. Am. 143 (3), http://dx.doi.org/10.1121/1.5036176, 1898–1898.

Strimbu, C.E., Olson, E.S., 2022. Salicylate-induced changes in organ of Corti vibrations. Hear. Res. 423, 108389.

Strimbu, C.E., Olson, E.S., 2025. Low-side and multi-tone suppression in the base of the gerbil cochlea. Biophys. J. http://dx.doi.org/10.1016/j.bpj.2024.12.004.

Strimbu, C.E., Wang, Y., Olson, E.S., 2020. Manipulation of the endocochlear potential reveals two distinct types of cochlear nonlinearity. Biophys. J. 119 (10), 2087–2101. http://dx.doi.org/10.1016/j.bpj.2020.10.005.

Von Békésy, G., Wever, E.G., 1960. Exeperiments in Hearing. McGraw-Hill.

Yoon, Y.-J., Steele, C.R., Puria, S., 2011. Feed-forward and feed-backward amplification model from cochlear cytoarchitecture: An interspecies comparison. Biophys. J. 100 (1), 1–10. http://dx.doi.org/10.1016/j.bpj.2010.11.039.